Supporting Information for

Metal fluorophosphate polyanionic insertion hosts as efficient bifunctional electrocatalysts for oxygen evolution and reduction reactions

Lalit Sharma,[a] Neha Bothra,[b] Rajeev Kumar Rai,[c] Swapan K. Pati,[b] and Prabeer Barpanda*[a]

[a] *Faraday Materials Laboratory (FaMaL), Materials Research Centre, Indian Institute of Science, C. V. Raman Avenue, Bangalore 560012, India*

[b] *Advanced Quantum Theory: Molecules to Materials Group, School of Advanced Materials (SAMat), Theoretical Science Unit, Jawaharlal Nehru Centre for Advanced Scientific Research, Jakkur, Bangalore 560064, India*

[c] *Materials Research Center, Indian Institute of Science, C. V. Raman Avenue, Bangalore 560012, India*

*author for correspondence
E-mail: prabeer@iisc.ac.in
Phone: +91-80 2293 2783; Fax: +91-80 2360 7316

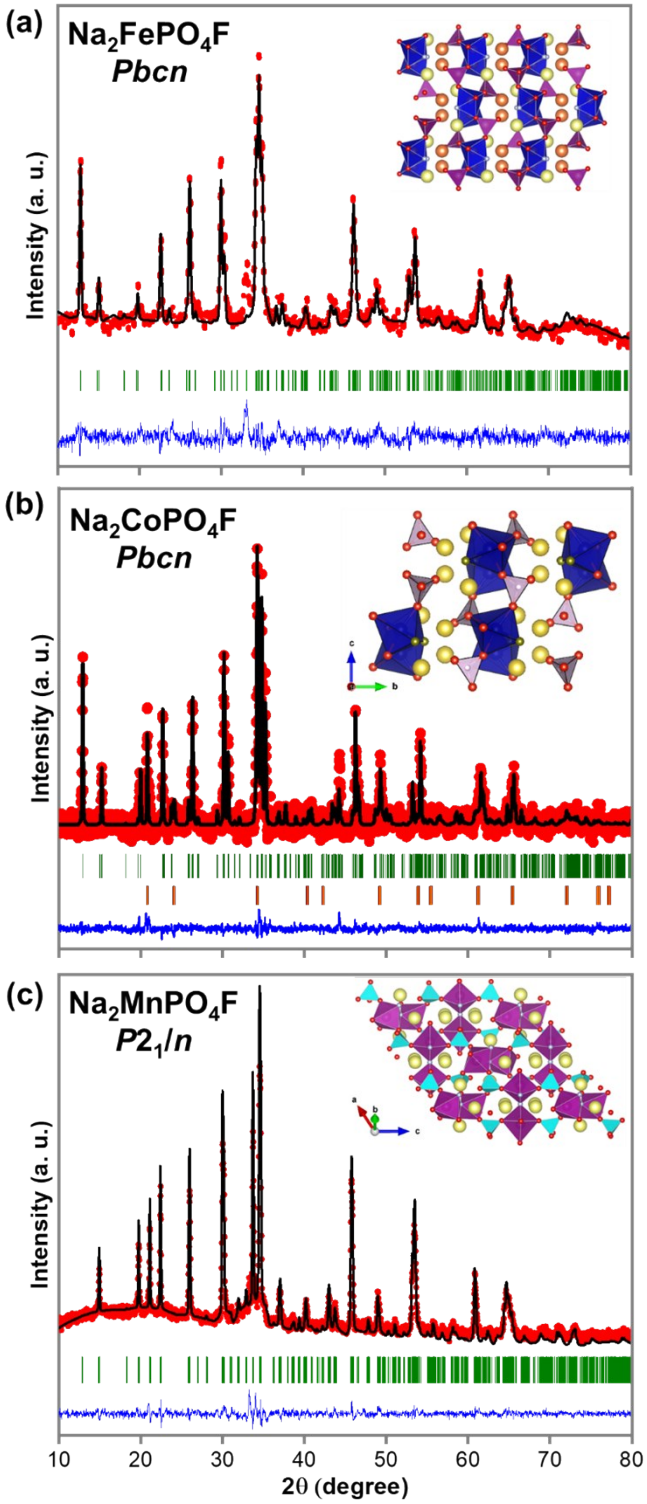

Fig. S1 Rietveld refinement of high resolution X-ray diffraction patterns (λ= 1.5418 Å) of (a) Na_2FePO_4F, (b) Na_2CoPO_4F and (c) Na_2MnPO_4F synthesized at 600 ^oC in 6 hours respectively. The experimental data points (red dots), calculated diffraction pattern (black line), their difference (blue line) and the Bragg positions (green ticks) are shown. Inset: (Right) Corresponding crystal structure of the fluorophosphate materials.

Table S1. Crystallographic data, lattice parameter and atomic coordinates of Na_2FePO_4F compound derived from Rietveld refinement.

Na_2FePO_4F

Formula Weight	Na_2FePO_4F [215.79 g mol^{-1}]
Temperature (K)	298
Crystal System	Orthorhombic
Space group	*Pbcn*
Unit cell parameter (Å)	a = 5.206(5), b = 13.810(0), c = 11.755(5)
	$\alpha = \beta = \gamma = 90^o$
Unit cell volume ($Å^3$)	845.8(3)
Fitness parameters (R values)	Rp = 9.09, Rwp = 9.302, χ^2 = 2.42

Atoms	**X**	**y**	**Z**	**Occ.**	**U_{iso}($Å^2$)**	**Wykoff position**
Fe1	0.24030	0.01310	0.32550	1	0.000	8d
P1	0.20890	0.38740	0.08360	1	0.004	8d
Na1	0.24300	0.24980	0.32610	1	1.000	8d
Na2	0.26200	0.12610	0.07800	1	0.000	8d
F1	0.00000	0.12550	0.25000	1	1.000	4c
F2	0.50000	0.10390	0.25000	1	1.000	4c
O1	0.25700	0.38750	-0.04280	1	1.000	8d
O2	0.27750	0.27960	0.13590	1	1.000	8d
O3	-0.08430	0.39470	0.10020	1	1.000	8d
O4	0.33950	0.46730	0.15150	1	1.000	8d

Table S2. Crystallographic data, lattice parameter and atomic coordinates of Na_2CoPO_4F compound derived from Rietveld refinement.

Na_2CoPO_4F

Formula Weight	Na_2CoPO_4F [218.88 g mol^{-1}]
Temperature (K)	298
Crystal System	Orthorhombic
Space group	*Pbcn*
Unit cell parameter (Å)	a = 5.246(4), b = 13.785(3), c = 11.677(5)
	$\alpha = \beta = \gamma$= 90º, Z = 8
Unit cell volume ($Å^3$)	844.5(7)
Fitness parameters (R values)	Rp = 3.24, Rwp = 6.53, χ^2 = 3.683

Atoms	**X**	**y**	**Z**	**Occ.**	**U_{iso}($Å^2$)**	**Wykoff position**
Co1	0.2413(0)	0.4819(6)	0.6722(7)	1	0.012	8d
P1	-0.2865(8)	0.6177(9)	0.5928(3)	1	0.093	8d
Na1	0.2543(1)	0.6353(9)	0.4189(9)	1	0.019	8d
Na2	0.2484(8)	0.2484(5)	0.6682(3)	1	0.048	8d
F1	0.5000(0)	0.3963(8)	0.7500(0)	1	0.101	4c
F2	0	0.3772(8)	0.7500(0)	1	0.203	4c
O1	-0.2073(4)	0.5406(9)	0.6754(7)	1	0.074	8d
O2	-0.2370(4)	0.7216(7)	0.6238(4)	1	0.016	8d
O3	0.4136(6)	0.6130(8)	0.5967(5)	1	0.036	8d
O4	0.2327(7)	0.3872(1)	0.5355(1)	1	0.043	8d

Table S3. Crystallographic data, lattice parameter and atomic coordinates of Na_2MnPO_4F compound derived from Rietveld refinement.

Na_2MnPO_4F

Formula Weight	Na_2MnPO_4F [214.89 g mol^{-1}]
Temperature (K)	298
Crystal System	Monoclinic
Space group	$P2_1/n$
Unit cell parameter (Å)	a = 13.69(3), b = 5.31(5), c = 13.71(7)
	$\alpha = \gamma = 90^o$, β =119.67, Z = 8
Unit cell volume ($Å^3$)	867.2(4)
Fitness parameters (R values)	Rp = 6.42, Rwp = 4.38, χ^2 = 2.23

Atoms	**X**	**y**	**Z**	**Occ.**	**U_{iso}($Å^2$)**	**Wykoff position**
Mn1	0.0925(3)	0.2732(3)	0.6761(2)	1	0.010	4e
Mn2	0.3259(9)	0.2330(0)	0.4020(0)	1	0.008	4e
P1	0.0807(1)	0.2121(2)	0.4154(5)	1	0.007	4e
P2	0.4148(9)	0.7119(9)	0.5788(8)	1	0.006	4e
Na1	0.5817(7)	0.2278(8)	0.6739(9)	1	0.013	4e
Na2	0.1718(9)	0.7527(7)	0.5877(7)	1	0.013	4e
Na3	0.3331(1)	0.2519(9)	0.6679(9)	1	0.013	4e
Na4	0.1629(1)	0.7298(9)	0.3291(1)	1	0.013	4e
F1	0.2251(1)	0.0027(7)	0.2367(7)	1	0.010	4e
F2	0.2464(5)	-0.0024(4)	0.7585(6)	1	0.011	4e
O1	0.3420(0)	0.8296(6)	0.4444(4)	1	0.011	4e

O2	0.1459(9)	0.3146(6)	0.5477(7)	1	0.013	4e
O3	-0.0330(0)	0.3515(5)	0.3541(1)	1	0.011	4e
O4	0.4186(6)	0.4155(6)	0.5799(0)	1	0.011	4e
O5	0.5377(8)	0.8177(8)	0.6368(8)	1	0.012	4e
O6	0.3435(6)	0.7679(9)	0.6400(1)	1	0.013	4e
O7	0.0683(3)	-0.0724(0)	0.4112(3)	1	0.012	4e
O8	0.1513(4)	0.2699(0)	0.3590(0)	1	0.012	4e

Table S4: ORR/OER electrocatalytic performance of various reported (non-noble metal-based) bifunctional materials.

Catalyst	Loading (mg cm^{-2})	$E_{1/2, ORR}$ (V vs. RHE)	$E_{OER, J=10\ mA\ cm-2}$ (V vs. RHE)	ΔE (V vs. RHE)	Reference
$NiCo_2O_4$	0.15	0.75	1.55	0.8	1
$MnCo_2O_4$	0.20	0.8	1.63	0.83	2
$Mn_xCo_{3-x}O_4$@NCNTs	0.28	0.76	1.70	0.94	3
MnO@Co-N/C	0.134	0.83	1.76	0.93	4
$CoMnPO_4$@P, N Co-doped carbon	0.30	0.81	1.56	0.75	5
$CuCo_2S_4$ NSs	-	0.74	1.567	0.835	6
Co_9S_8/CNT	-	0.82	1.599	0.779	7
$CoMn_2O_4$ porous microspheres	0.051	0.75	1.83	1.08	8
Fe doped CoV_2O_4	0.198	0.66	1.53	0.87	9
5% Ni doped Co_3O_4	0.408	0.83	1.61	0.78	10
$NiMnO_3/NiMn_2O_4$ heterojunction	0.24	0.75	1.61	0.86	11
$Co_2P_2O_7$/NPGA	0.20	0.80	1.57	0.77	12
$Co_3FeS_{1.5}(OH)_6$	0.255	0.721	1.588	0.867	13
Co-N@HCS	1.52	0.864	1.72	0.856	14
$CuCo_2O_4$/N-CNTs	0.20	0.798	1.699	0.901	15
$NaCoPO_4$*	0.398	0.69	1.61	0.92	16
$Na_2CoP_2O_7$*	0.398	0.70	1.59	0.89	16
Na_2FePO_4F	0.398	0.770	1.80	1.03	Present work
Na_2CoPO_4F	0.398	0.831	1.73	0.899	Present work
Na_2MnPO_4F	0.398	0.845	-	-	Present work

* Electrolyte: 1 M NaOH; E_{ORR} @ -1 mA cm^{-2}

References:

1 J. Zhao, Y. He, Z. Chen, X. Zheng, X. Han, D. Rao, C. Zhong, W. Hu and Y. Deng, Engineering the surface metal active sites of nickel cobalt oxide nanoplates toward enhanced oxygen electrocatalysis for Zn-air battery, *ACS Appl. Mater. Interfaces*, 2019, **11**, 4915-4921.

2 W. Wang, L. Kuai, W. Cao, M. Huttula, S. Ollikkala, T. Ahopelto, A. P. Honkanen, S. Huotari, M. Yu and B. Geng, Mass-production of mesoporous $MnCo_2O_4$ spinels with Manganese(IV)- and cobalt(II)-rich surfaces for superior bifunctional oxygen electrocatalysis, *Angew. Chem. Int. Ed.*, 2017, **129**, 15173-15177.

3 T. Zhao, S. Gadipelli, G. He, M. J. Ward, D. Do, P. Zhang and Z. Guo, Tunable bifunctional activity of $Mn_xCo_{3-x}O_4$ nanocrystals decorated on carbon nanotubes for oxygen electrocatalysis, *ChemSusChem*, 2018, **11**, 1295-1304.

4 Y. Chen, Y. Guo, H. Cui, Z. Xie, Z. Xin, J. Wei and Z. Zhen, Bifunctional electrocatalysts of MOF-derived Co-N/C on bamboo-like MnO nanowires for high-performance liquid-state and solid-state Zn-air batteries, *J. Mater. Chem. A*, 2018, **6**, 9716-9722.

5 S. Yang, Q. He, C. Wang, H. Jiang, C. Wu, Y. Zhang, T. Zhou, Y. Zhou and L. Song, Confined bimetallic phosphide within P, N co-doped carbon layers towards boosted bifunctional oxygen catalysis, *J. Mater. Chem. A*, 2018, **6**, 11281-11287.

6 S. Zhao, Y. Wang, Q. Zhang, Y. Li, L. Gu, Z. Dai, S. Liu, Y. Q. Lan, M. Han and J. Bao, Two-dimensional nanostructures of non-layered ternary thiospinels and their bifunctional electrocatalytic properties for oxygen reduction and evolution: the case of $CuCo_2S_4$ nanosheets, *Inorg. Chem. Front.*, 2016, **3**, 1501-1509.

7 H. Li, Z. Guo and X. Wang, Atomic-layer-deposited ultrathin Co_9S_8 on carbon nanotubes: an efficient bifunctional electrocatalyst for oxygen evolution/reduction reactions and rechargeable Zn-air batteries, *J. Mater. Chem. A*, 2017, **5**, 21353-21367.

8 P. W. Menezes, A. Indra, N. R. Sahraie, A. Bergmann, P. Strasser and M. Driess, Cobalt-manganese-based spinels as multifunctional materials that unify catalytic water oxidation and oxygen reduction reactions, *ChemSusChem*, 2015, **8**, 164-171.

9 K. Chakrapani, G. Bendt, H. Hajiyani, T. Lunkenbein, M. T. Greiner, L. Masliuk, S. Salamon, J. Landers, R. Schlogl, H. Wende, R. Pentcheva, S. Schulz and M. Behrens, The role of composition of uniform and highly dispersed cobalt vanadium iron spinel nanocrystals for oxygen electrocatalysis, *ACS Catal.*, 2018, **8**, 1259-1267.

10 W. Song, Z. Ren, S. Y. Chen, Y. Meng, S. Biswas, P. Nandi, H. A. Elsen, P. X. Gao and S. L. Suib, Ni- and Mn-promoted mesoporous Co_3O_4: A stable bifunctional catalyst with surface-structure-dependent activity for oxygen reduction reaction and oxygen evolution reaction, *ACS Appl. Mater. Interfaces*, 2016, **8**, 20802-20813.

11 X. He, F. Yin, Y. Li, H. Wang, J. Chen, Y. Wang and B. Chen, $NiMnO_3/NiMn_2O_4$ oxides synthesized via the Aid of pollen: Ilmenite/spinel hybrid nanoparticles for highly efficient bifunctional oxygen electrocatalysis, *ACS Appl. Mater. Interfaces*, 2016, **8**, 26740-26757.

12 J. T. Ren, G. G. Yuan, L. Chen, C. C. Weng and Z. Y. Yuan, 2D cocrystallized metal-organic nanosheet array as an efficient and stable bifunctional electrocatalyst for overall water splitting, *ACS Sustainable Chem. Eng.*, 2018, **6**, 9793-9803.

13 H. F. Wang, C. Tang, B. Wang, B. Q. Li and Q. Zhang, Bifunctional transition metal hydroxysulfides: room-temperature sulfurization and their applications in Zn-air batteries, *Adv. Mater.*, 2017, **29**, 1702327.

14 H. Fan, H. Yu, Y. Zhang, Y. Zheng, Y. Luo, Z. Dai, B. Li, Y. Zong and Q. Yan, Fe-doped Ni_3C nanodots in N-doped carbon nanosheets for efficient hydrogen-evolution and oxygen-evolution electrocatalysis, *Angew. Chem. Int. Ed.*, 2017, **56**, 12566-12570.
15 H. Cheng, M. L. Li, C. Y. Su, N. Li and Z. Q. Liu, Cu-Co bimetallic oxide quantum dot decorated nitrogen-doped carbon nanotubes: A high-efficiency bifunctional oxygen electrode for Zn-air batteries, *Adv. Funct. Mater.*, 2017, **27**, 1702327.
16 R. Gond, K. Sada, B. Senthilkumar and P. Barpanda, Bifunctional electrocatalytic behavior of sodium cobalt phosphates in alkaline solution, *ChemElectroChem*, 2018, **5**, 153-158.

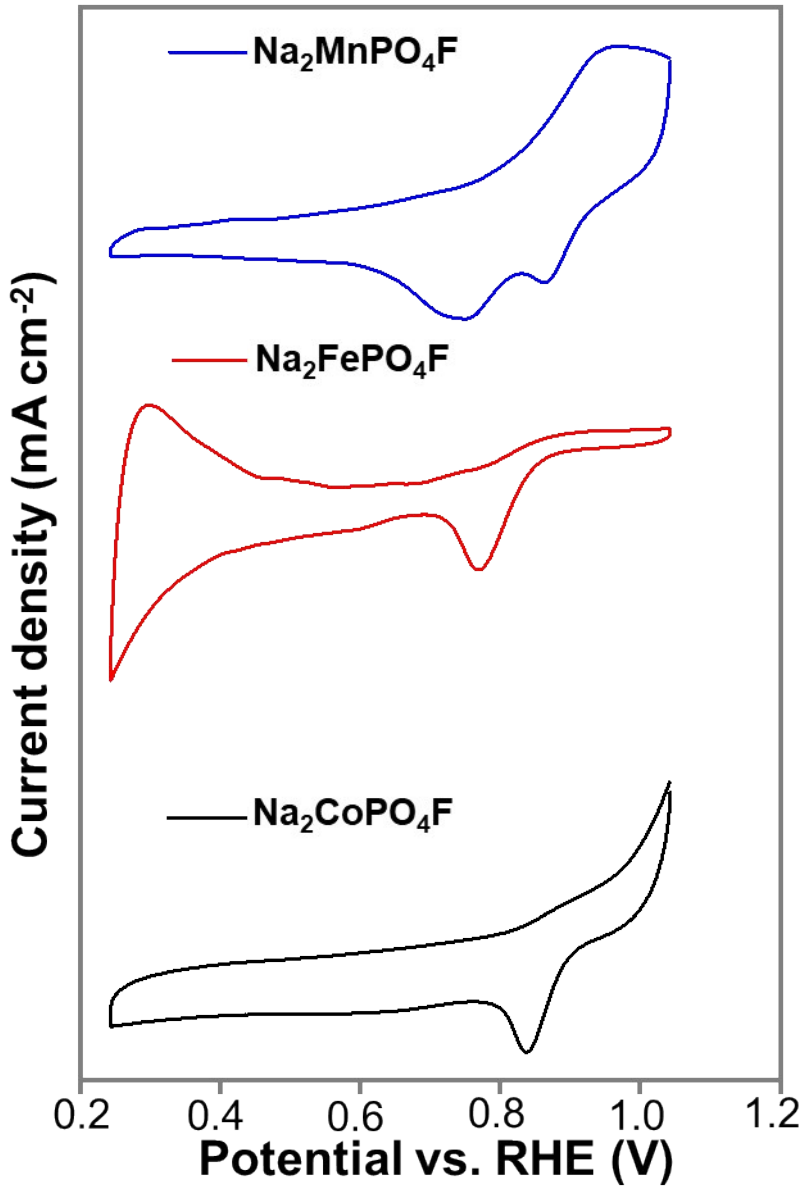

Fig. S2 Cyclic voltammograms of Na_2FePO_4F, Na_2CoPO_4F and Na_2MnPO_4F (for ORR process) recorded in alkaline medium (0.1 M KOH) in the voltage range of 0.1 to -0.7 V vs. Hg/HgO (later scaled to RHE).

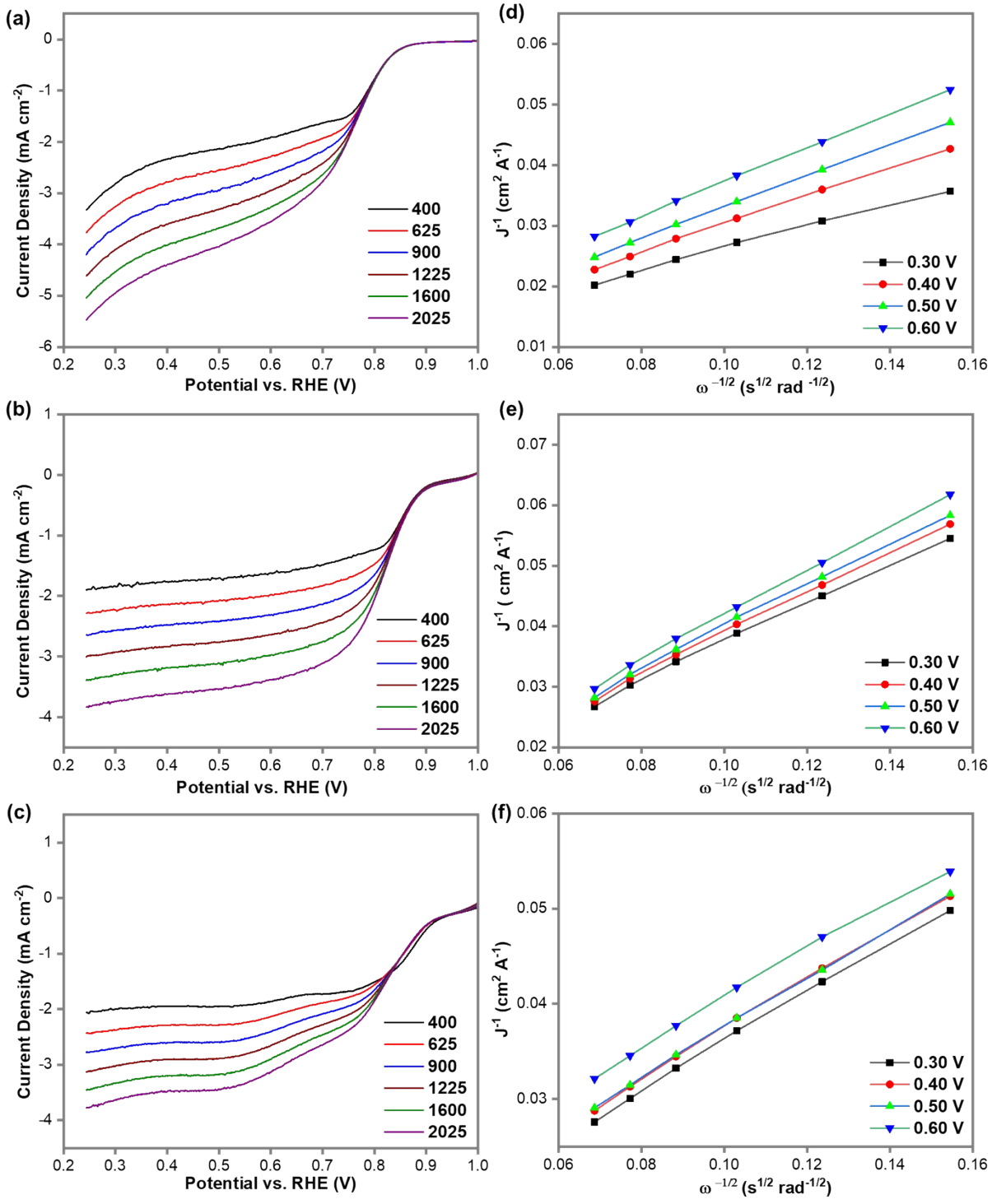

Fig. S3 Linear sweep voltammograms for ORR process recorded at different rotations per minute (rpm) and corresponding Koutecky-Levich (K-L) plots for (a, d) Na_2FePO_4F, (b, e) Na_2CoPO_4F, and Na_2MnPO_4F respectively.

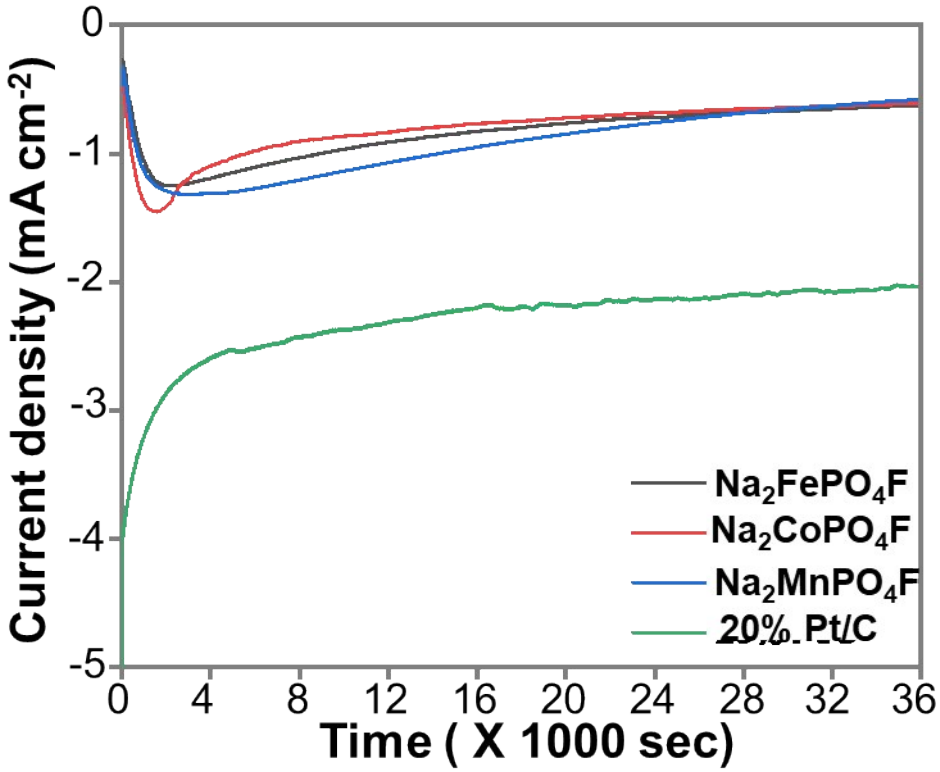

Fig. S4 Stability test of Na_2FePO_4F, Na_2CoPO_4F, Na_2MnPO_4F and 20% Pt/C recorded for 10 hours using chronoamperometry technique.

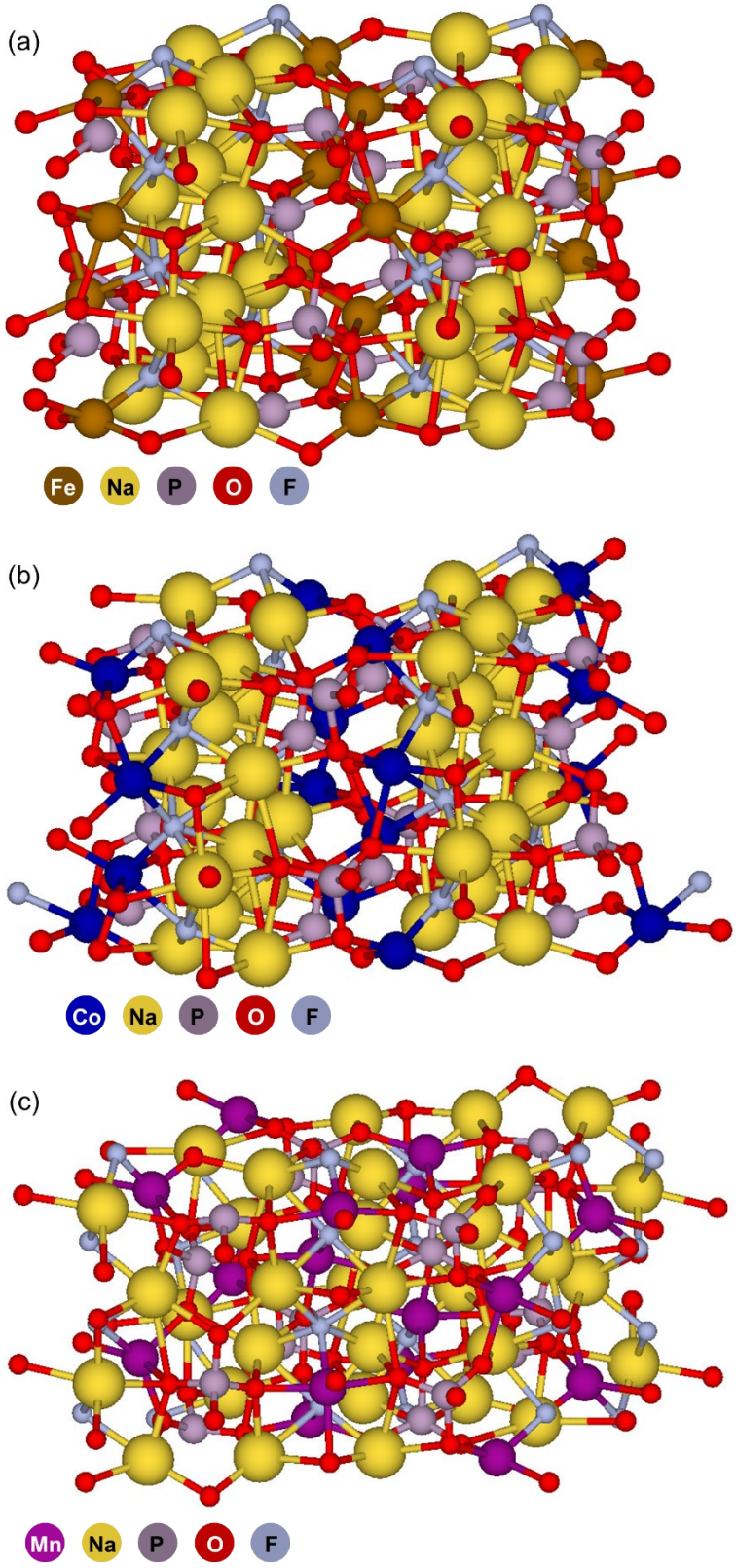

Fig. S5 The (100) active surface for (a) Na_2FePO_4F, (b) Na_2CoPO_4F and (010) active surface for (c) Na_2MnPO_4F used for theoretical calculations.

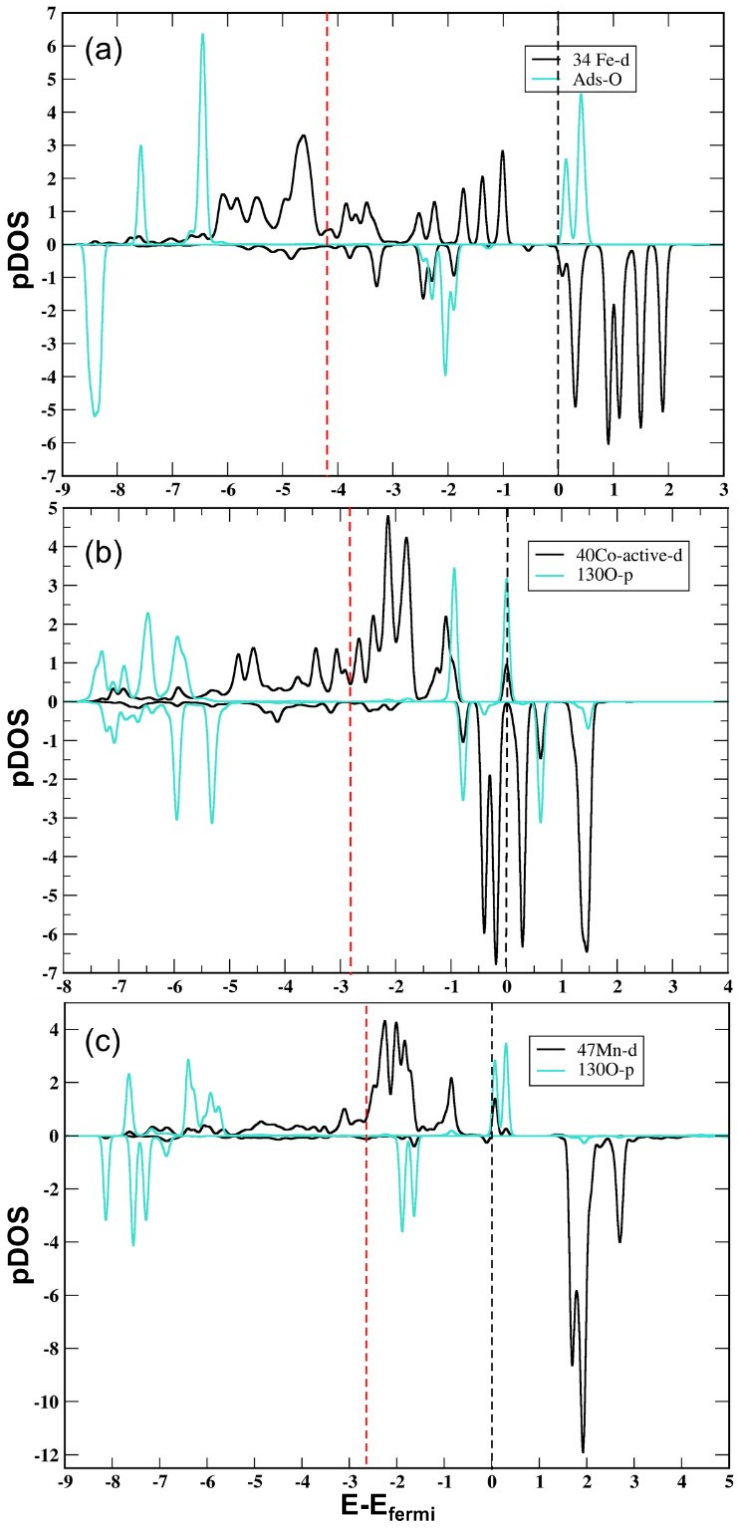

Fig. S6 Density of states (DOS) showing extent of overlapping of *d* orbitals of 3-d transition metal atom and adsorbed oxygen atom for (a) Na_2FePO_4F, (b) Na_2CoPO_4F and (c) Na_2MnPO_4F fluorophosphates respectively.